SAR Based Machine/Deep Learning Models for Sea Ice Surface Roughness and Thickness Predictions

1. Introduction

Numerous studies emphasize the importance of sea ice surface roughness and thickness estimations in various domains such as the navigation/exploration in sea ice regions (Karvonen, 2012b; Su et al., 2018), earth science research (Cafarella et al., 2018; Petty et al., 2020) and climate change research (Kim et al., 2011; Kwok et al., 2009; Lee et al., 2016; Liu et al., 2015). While such studies have contributed to the utilization of remote sensing data to detect sea ice features by finding correlation and statistical models, not many explored state-of-the-art compute-intensive methods such as Machine/Deep Learning architectures. Furthermore, many previous studies have taken advantage of precise high-resolution data that are often privately accessible, leading to poor practicality. Other limitations to such data are small coverage and temporal resolution. This project aims to develop Machine/Deep Learning architectures to mitigate such constraints by using abundant spaceborne RADARSAT-2 Synthetic Aperture Radar (SAR) data for sea ice surface roughness and thickness predictions. The literature review intends to provide background knowledge and relevant studies that would potentially assist the project in producing quality results.

2. Attempts on Sea Ice Surface Roughness and Thickness prediction

SAR data are sensitive to surface roughness, and the characteristic allowed researchers to utilize them in sea ice research. Cafarella et al. (2019) have taken account of RADARSAT-2 and ALOS-2 PALSAR-2 SAR data to estimate the surface roughness of deformed first-year ice in the Canadian arctic archipelago. According to their study, surface roughness variations smaller than the microwave wavelength significantly impact SAR backscatter intensity. Therefore, radar frequency is an important control factor of the surface scattering mechanism. Millimetres to centimetre scale surface roughness from first-year ice (FYI) and air bubbles in multi-year ice (MYI) can be detected with the C-band (Cafarella et al., 2019), which is the same frequency range of the data used for this project. The experiment results by Cafarella et al. (2019) suggest a high positive correlation (r=0.86) between C-band HH-polarization backscatter and FYI roughness in winter. Furthermore, a strong negative correlation

with Pearson's r-value of -0.83 was observed for FYI roughness estimation in the advanced melt season using HV/HH ratio feature. All data were collected at a shallow incidence angle. The promising results suggest using the backscattering features to train this project's output model will result in high surface roughness prediction accuracy.

Multiple studies have been utilizing laser and radar altimetry data collected from ICESat and CryoSat missions, respectively, for sea ice thickness analyses (Kwok et al., 2009; Lee et al., Landy et al. 2020; 2016; Petty et al., 2020). Kwok et al. (2009) and Petty et al. (2020) have devised methods to estimate sea ice thickness derived from its isostatic equilibrium and freeboard measured using ICESat and ICESat-2 data. The accuracy of such techniques highly depends on lead identification precision, which is a primary weakness of the approach. To overcome the problem, Lee et al. (2016) experimented with machine learning approaches of decision trees and random forests to improve lead detection accuracy for sea ice thickness prediction. The method recorded a Root Mean Square Error (RMSE) of 0.3 m when compared with the expert airborne electromagnetic (AEM) data. It is a significant improvement from an RMSE of 0.9 m using the previous thresholding lead detection method. Nevertheless, no further attempts were made to use Machine/Deep Learning architectures to solve the regression problem. Landy et al. (2020) suggested a potential feature, roughness, as a critical factor in estimating sea ice freeboard with CryoSat-2 data. The feature has been ignored or misrepresented in other studies. They claim, by disregarding the roughness feature in the estimation, the potential error could range up to 20% over first-year ice (FYI) and 30% over multi-year ice (MYI). Although the project does not take advantage of the high-resolution CryoSat data, it might be helpful to take account of the roughness results for the thickness prediction.

While it is not the most popular approach to estimate sea ice thickness with spaceborne SAR data, there have been several attempts to accomplish the task. Kim et al. (2012) discovered a potential one-to-one correlation between the fast sea ice thickness and depolarization factors: co-polarized correlation and cross-polarization ratio. The correlation coefficients ranged from 0.76 to 0.88 regardless of the sea ice types using the C and X bands collected from TerraSAR-X and RADARSAT-2 missions.

A study by Karvonen et al. (2012b) further created a sea ice thickness estimation model with high accuracy obtained using SAR data from RadarSat missions. The algorithm developed for the study is assisted by the thickness product of a sea ice thermodynamic snow/ice model, called HIGHTSI, and uses additional information of the SAR features, ice concentration and ice drift. The HIGHTSI simulations require high-resolution atmospheric forcing, which is not provided in this project. However, the study offers various useful SAR-based features for sea ice thickness prediction, and they are covered in the next section. The algorithm outperformed the standalone HIGHTSI method and Canadian Ice Service (CIS) ice chart estimations with 5.5% and 23.9% thickness errors for training and test accuracies. Nevertheless, the problem of the model's incapability of locating thin ice remains. The studies in this paragraph argue that promising sea ice thickness prediction results can be obtained from using SAR features.

3. Data Preprocessing

3.1. Pixel-based method

As discussed in the previous section, the amount of backscattered microwaves is highly dependent on the surface roughness and is represented well in SAR data. To propagate such information, multiple sea ice studies use Gray-Level Co-occurrence Matrix (GLCM) products to extract additional SAR texture features (Liu & Zhang, 2010; Ressel et al., 2015). A square-shaped sliding window is required to generate GLCMs. For each window, the frequency histogram of every possible adjacent pixel value pair is recorded in the form of a two-dimensional matrix, where each axis represents the relative location within the pair (e.g. north-south, west-east, NE-SW, etc.). There are numerous GLCM products, such as the mean, variance, homogeneity, contrast, dissimilarity, entropy, angular second moment, and correlation (Liu & Zhang, 2010). Still, Ressel et al. (2015) utilized five of them for their study:

$$Entropy = -\sum_{i=1}^{n}\sum_{j=1}^{n} GLCM[i][j] \times log(GLCM[i][j]) \quad (1)$$

$$Energy\ (ASM) = \sum_{i=1}^{n}\sum_{j=1}^{n} GLCM[i][j]^2 \quad (2)$$

$$Contrast = \sum_{i=1}^{n}\sum_{j=1}^{n} |i-j|^2 \times GLCM[i][j] \quad (3)$$

$$Homogeneity = \sum_{i=1}^{n}\sum_{j=1}^{n} \frac{GLCM[i][j]}{1+(i-j)^2} \quad (4)$$

$$Dissimilarity = \sum_{i=1}^{n}\sum_{j=1}^{n} GLCM[i][j] \times |i-j| \quad (5)$$

Where n×n = GLCM size and (i, j) = coordinates in GLCM. Although the studies included in this paragraph aim at an objective different from this project, sea ice type classification is interactively related to sea ice thickness estimation (Kim et al., 2012; Karvonen et al., 2012b). No or small negative influences are expected when the GLCM products are fed into the training process.

Gradient features extracted from SAR data detect edges in an image. Helpful information on the ice deformation and structure can be derived from them (Karvonen et al.,2012a). They can also be used to estimate sea ice concentration, which is then fed into a sea ice thickness prediction model (Karvonen et al.,2012b). The extraction steps are as follows: 1) absolute gradient calculation over the whole image, 2) thresholding pixels within a 5-pixel radius circular window, and 3) gradient feature calculation. For the first step, Canny edge detection is better at absolute gradient approximation than Sobel detection (Ahmed, 2018; Vijayarani & Vinupriya, 2013). The second step involves the expectation-maximization (EM) clustering and the bayesian criteria to find the optimal threshold. Once the relative high gradient and low gradient pixels are identified, five features are calculated (Karvonen et al.,2012a):

$$GF_1 = N_h/N \quad (6)$$

$$GF_2 = T \quad (7)$$

$$GF_3 = \sqrt{\lambda_1/\lambda_2} \quad (8)$$

$$GF_4 = m_2 - m_1 \quad (9)$$

$$GF_5 = N_{hf}/N \quad (10)$$

where N=total number of pixels in a window, N_h = the number of high-gradient pixels, T = optimal threshold, (λ_1, λ_2) = two eigenvalues of the covariance matrix of the locations

of the high-gradient pixels, m_2-m_1 = euclidean distance between peaks of high-gradient and low-gradient pixel distributions, and N_{hf} = number of filtered high-gradient pixels. Karvonen et al. (2012b) used GF_1, GF_2 and GF_3 for their sea ice concentration and thickness estimation algorithm mentioned in section 2.

3.2. Object-based method

According to several studies (Liu and Xia, 2010; Wan et al., 2019), the object-based approach is often preferred over the pixel-based method in remote sensing to remove the salt-and-pepper effects in the classification result. An object-based method is also advantageous by having more features that can characterize the object's spatial, textural and contextual properties along with the original spectral information. However, the performance of object-based classification in remote sensing depends on the segmentation scales. Under-segmentation occurs when an object includes more than one class but is assigned to the same class. It can result in a lower accuracy than pixel-based classification (Liu and Xia, 2010). This issue should be addressed, and experiments are needed to find the optimal scale.

Segment-wise SAR texture feature extraction method for sea ice thickness estimation was suggested by Karvonen et al. (2012b**)** based on the assumption that more substantial texture reflects the characteristics of older and thicker ice on a local scale. The coefficient of variation describes such texture feature:

$$C_v = 100\,\sigma(r, c) \,/\, \mu(r, c) \qquad (11)$$

Where μ(r, c) = mean of values in the segment having the pixel at (r, c), and σ(r, c) = standard deviation within the object having the pixel at (r, c).

3.3. Normalization

Normalizing the features is a common Machine Learning practice to enhance the model performance, and Zhang et al. (2015) researched this topic with optical and SAR data fusion. They experimented with three normalization approaches with output scales of [-1, 1], [0, 255] and [0, 1]. The conversion from a datum, x, to its normalized value, y, is as below:

$$y = (y_{max} - y_{min})\frac{x - x_{min}}{x_{max} - x_{min}} + y_{min} \qquad (12)$$

Where (x_{min}, x_{max}) is the minimum-maximum value pair in the original data, and (y_{min}, y_{max}) is the minimum-maximum value pair in the normalization scale. No significant impacts were observed when normalized data were applied to land-use/land-cover (LULC) classification with Maximum Likelihood (ML) and Support Vector Machine (SVM) methods. The Minimum Distance (MD) method was influenced positively by feature normalization, improving accuracy from 75.94% to 82.85%. However, Artificial Neural Networks (ANN) seemed sensitive to normalized input features depending on the normalization scale. In general, decreased accuracy on ANN was recorded after normalization. The authors did not identify the exact reasons that caused an unexpected result and suggested more experiments are required to find an optimal normalization strategy.

4. Machine/Deep Learning Strategies

4.1. Feature Engineering with Autoencoder

A previous study experimented with the sparse autoencoder (SAE) feature engineering for three-class (open water, thick ice and thin ice) classification of sea ice thickness using optical unmanned aerial vehicle (UAV) (Su et al., 2018). The architecture involves SAE for first- and second-order feature generations, and the final features are fed into the softmax classifier (Figure 1).

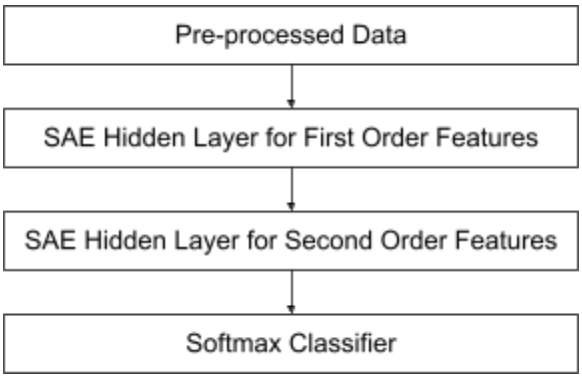

Figure 1. Illustration of a softmax classification with SAE feature engineering.

Better accuracy was obtained with the increasing number of training samples in general. Test accuracy ranged from 74.02% to 95.25% when trained with 1.1 million samples, while 0.3 million samples resulted in the range of 71.94% to 93.23%. It is

expected that SAE would not be required for pixel-based learning due to a low complexity in feature space. However, the usefulness of the autoencoder architecture is emphasized when the complexity grows when data are combined as objects.

4.2. Semi-supervised Learning

The key objective of this project is to develop a deep learning model using SAR data instead of AEM data. The labelled expert AEM data are collected at a higher cost causing a smaller amount and coverage than the large unlabelled SAR training dataset. There might be a potential problem having an insufficient number of expert data for proper training. Vatasavai et al. (2007) addressed the issue of the growing amount of remote sensing data with a small number of labelled training data. They devised EM-based spatial semi-supervised learning (SSSL) algorithms to solve the problem. Maximum Likelihood and Maximum a posteriori classifiers are used (MLC and MAP). The researchers also attempted to take account of spatial dependencies, such as spatial context and autocorrelation, through Markov Random Fields (MRF). A generalized description of SSSL consists of three main steps: 1) initial generation of the classifier using labelled data, 2) using the initial classifier to estimate the class membership of all samples, and 3) the final generation of the classifier given samples and a neighbourhood model calculated using the Gaussian mixture component membership. In the second step, class memberships are represented in the probability that sample points are generated through the Gaussian mixture model. The SSSL outperformed with a 12% improvement from the 60% classification accuracy obtained using a basic model trained solely with step 1). A standard semi-supervised algorithm without step 3) and an MRF model trained without step 2) recorded 68% and 65%, respectively. Despite the study being conducted to solve a classification problem, the performance enhancements using such methods, especially SSSL, are significant enough to be considered to deploy them in this project's regression problem. Their compatibility with regression problems, which is likely to require changes in the algorithm regarding the statistical methods, should be checked. However, the paper was published before the ANN gained its popularity in the early 2010s. The accuracy achieved using SSSL might not be satisfactory compared to a model trained by regular deep learning strategies. Nevertheless, the general idea of semi-supervised learning

coupled with deep learning strategies might be a candidate for the performance enhancement of object-based regression. The MRF method for feeding local spatial context into the estimation should also be considered.

References

Ahmed, A. S. (2018). Comparative study among Sobel, Prewitt and Canny edge detection operators used in image processing. J. Theor. Appl. Inf. Technol, 96(19), 6517-6525.

Cafarella, S. M., Scharien, R., Geldsetzer, T., Howell, S., Haas, C., Segal, R., & Nasonova, S. (2019). Estimation of Level and Deformed First-Year Sea Ice Surface Roughness in the Canadian Arctic Archipelago from C- and L-Band Synthetic Aperture Radar. Canadian Journal of Remote Sensing, 45(3–4), 457–475. https://doi.org/10.1080/07038992.2019.1647102

Karvonen, J., & Chen, C. H. (2012a). NMF and NTF for sea ice SAR feature extraction and classification. Signal and Image Processing for Remote Sensing, 2nd edition, edited by: Chen, CH, CRC Press, Boca Raton, FL. USA, 117-128.

Karvonen, J., Cheng, B., Vihma, T., Arkett, M., & Carrieres, T. (2012b). A method for sea ice thickness and concentration analysis based on SAR data and a thermodynamic model. The Cryosphere, 6(6), 1507–1526. https://doi.org/10.5194/tc-6-1507-2012

Kim, J. W., Kim, D. J., & Hwang, B. J. (2012). Characterization of Arctic Sea Ice Thickness Using High-Resolution Spaceborne Polarimetric SAR Data. IEEE Transactions on Geoscience and Remote Sensing, 50(1), 13–22. https://doi.org/10.1109/tgrs.2011.2160070

Kwok, R., Cunningham, G. F., Wensnahan, M., Rigor, I., Zwally, H. J., & Yi, D. (2009). Thinning and volume loss of the Arctic Ocean sea ice cover: 2003–2008. Journal of Geophysical Research, 114(C7). https://doi.org/10.1029/2009jc005312

Landy, J. C., Petty, A. A., Tsamados, M., & Stroeve, J. C. (2020). Sea Ice Roughness Overlooked as a Key Source of Uncertainty in CryoSat‐2 Ice Freeboard Retrievals. Journal of Geophysical Research: Oceans, 125(5). https://doi.org/10.1029/2019jc015820

Lee, S., Im, J., Kim, J., Kim, M., Shin, M., Kim, H. C., & Quackenbush, L. (2016). Arctic Sea Ice Thickness Estimation from CryoSat-2 Satellite Data Using Machine Learning-Based Lead Detection. Remote Sensing, 8(9), 698. https://doi.org/10.3390/rs8090698

Liu, H., Guo, H., & Zhang, L. (2015). SVM-Based Sea Ice Classification Using Textural Features and Concentration From RADARSAT-2 Dual-Pol ScanSAR Data. IEEE Journal of Selected Topics in Applied Earth Observations and Remote Sensing, 8(4), 1601–1613. https://doi.org/10.1109/jstars.2014.2365215

Liu, D., & Xia, F. (2010). Assessing object-based classification: advantages and limitations. Remote Sensing Letters, 1(4), 187–194. https://doi.org/10.1080/01431161003743173

Petty, A. A., Kurtz, N. T., Kwok, R., Markus, T., & Neumann, T. A. (2020). Winter Arctic Sea Ice Thickness From ICESat‐2 Freeboards. Journal of Geophysical Research: Oceans, 125(5). https://doi.org/10.1029/2019jc015764

Ressel, R., Frost, A., & Lehner, S. (2015). A Neural Network-Based Classification for Sea Ice Types on X-Band SAR Images. IEEE Journal of Selected Topics in Applied Earth Observations and Remote Sensing, 8(7), 3672–3680. https://doi.org/10.1109/jstars.2015.2436993

Su, N., Zhang, C., Yan, Y., Zhao, C., & Tan, Z. (2018). Sea-Ice Image Classification for Channel Navigation in Polar Application. IGARSS 2018 - 2018 IEEE International Geoscience and Remote Sensing Symposium. Published. https://doi.org/10.1109/igarss.2018.8518191

Vatsavai, R. R., Shekhar, S., & Burk, T. E. (2007). An efficient spatial semi-supervised learning algorithm. International Journal of Parallel, Emergent and Distributed Systems, 22(6), 427–437. https://doi.org/10.1080/17445760701207546

Vijayarani, S., & Vinupriya, M. (2013). Performance analysis of canny and sobel edge detection algorithms in image mining. International Journal of Innovative Research in Computer and Communication Engineering, 1(8), 1760-1767.

Wan, L., Zhang, T., & You, H. (2019). Object‐based method for optical and SAR images change detection. The Journal of Engineering, 2019(21), 7410–7414. https://doi.org/10.1049/joe.2019.0620

Zhang, H., Lin, H., & Li, Y. (2015). Impacts of feature normalization on optical and SAR data fusion for land use/land cover classification. IEEE Geoscience and Remote Sensing Letters, 12(5), 1061-1065. https://doi.org/10.1109/LGRS.2014.2377722